Research Article | Vol. 9, No. 4 | 1 Apr 2018 | BIOMEDICAL OPTICS EXPRESS 1893

Biomedical Optics EXPRESS

# Observation of laser-induced elastic waves in agar skin phantoms using a high-speed camera and a laser-beam-deflection probe

**JERNEJ LALOŠ,* PETER GREGORČIČ, AND MATIJA JEZERŠEK**

*Faculty of Mechanical Engineering, University of Ljubljana, Aškerčeva cesta 6, 1000 Ljubljana, Slovenia*
**jernej.lalos@fs.uni-lj.si*

**Abstract:** We present an optical study of elastic wave propagation inside skin phantoms consisting of agar gel as induced by an Er:YAG (wavelength of 2.94 μm) laser pulse. A laser-beam-deflection probe is used to measure ultrasonic propagation and a high-speed camera is used to record displacements in ablation-induced elastic transients. These measurements are further analyzed with a custom developed image recognition algorithm utilizing the methods of particle image velocimetry and spline interpolation to determine point trajectories, material displacement and strain during the passing of the transients. The results indicate that the ablation-induced elastic waves propagate with a velocity of 1 m/s and amplitudes of 0.1 mm. Compared to them, the measured velocities of ultrasonic waves are much higher, within the range of 1.42–1.51 km/s, while their amplitudes are three orders of magnitude smaller. This proves that the agar gel may be used as a rudimental skin and soft tissue substitute in biomedical research, since its polymeric structure reproduces adequate soft-solid properties and its transparency for visible light makes it convenient to study with optical instruments. The results presented provide an insight into the distribution of laser-induced elastic transients in soft tissue phantoms, while the experimental approach serves as a foundation for further research of laser-induced mechanical effects deeper in the tissue.

© 2018 Optical Society of America under the terms of the OSA Open Access Publishing Agreement

**OCIS codes:** (170.0170) Medical optics and biotechnology; (280.3375) Laser induced ultrasonics; (170.0110) Imaging systems; (100.3008) Image recognition, algorithms and filters; (040.1490) Cameras; (140.3500) Lasers, erbium.

## References and links

1. H.-P. Berlien and G. J. Müller, eds., *Applied Laser Medicine* (Springer-Verlag, 2003).
2. R. W. Waynant, ed., *Lasers in Medicine* (CRC Press, 2001).
3. K. Nouri, ed., *Lasers in Dermatology and Medicine* (Springer, 2011).
4. V. V. Tuchin, ed., *Handbook of Optical Biomedical Diagnostics, Second Edition, Volume 1: Light-Tissue Interaction* (SPIE Press, 2016).
5. V. V. Tuchin, ed., *Handbook of Optical Biomedical Diagnostics, Second Edition, Volume 2: Methods* (SPIE Press, 2016).
6. S. Choudhary, M. L. Elsaie, A. Leiva, and K. Nouri, "Lasers for tattoo removal: a review," Lasers Med. Sci. **25**(5), 619–627 (2010).
7. A. J. Welch and M. J. C. van Gemert, eds., *Optical-Thermal Response of Laser-Irradiated Tissue, Second Edition* (Springer Netherlands, 2011).
8. B. F. Kennedy, P. Wijesinghe, and D. D. Sampson, "The emergence of optical elastography in biomedicine," Nat. Photonics **11**(4), 215–221 (2017).
9. K. V. Larin and D. D. Sampson, "Optical coherence elastography - OCT at work in tissue biomechanics [Invited]," Biomed. Opt. Express **8**(2), 1172–1202 (2017).
10. B. F. Kennedy, K. M. Kennedy, and D. D. Sampson, "A Review of Optical Coherence Elastography: Fundamentals, Techniques and Prospects," IEEE J. Sel. Top. Quant. **20**(2), 272 (2014).
11. S. P. Kearney, A. Khan, Z. Dai, and T. J. Royston, "Dynamic viscoelastic models of human skin using optical elastography," Phys. Med. Biol. **60**(17), 6975–6990 (2015).
12. B. F. Kennedy, S. H. Koh, R. A. McLaughlin, K. M. Kennedy, P. R. T. Munro, and D. D. Sampson, "Strain estimation in phase-sensitive optical coherence elastography," Biomed. Opt. Express **3**(8), 1865–1879 (2012).
13. B. F. Kennedy, R. A. McLaughlin, K. M. Kennedy, L. Chin, A. Curatolo, A. Tien, B. Latham, C. M. Saunders, and D. D. Sampson, "Optical coherence micro-elastography: mechanical-contrast imaging of tissue microstructure," Biomed. Opt. Express **5**(7), 2113–2124 (2014).

#319600 https://doi.org/10.1364/BOE.9.001893
Journal © 2018 Received 11 Jan 2018; revised 6 Mar 2018; accepted 20 Mar 2018; published 26 Mar 2018

14. M. Doi, *Soft Matter Physics, 1st Edition* (Oxford University Press, 2013).
15. M. Kleman and O. D. Lavrentovich, *Soft Matter Physics, An Introduction* (Springer, 2003).
16. W. G. Pitt, G. A. Husseini, and B. J. Staples, "Ultrasonic drug delivery-a general review," Expert Opin. Drug Deliv. **1**(1), 37–56 (2004).
17. H. Jang, S. Yeo, and J. J. Yoh, "Synchronization of skin ablation and microjet injection for an effective transdermal drug delivery," Appl. Phys., A Mater. Sci. Process. **122**(4), 320 (2016).
18. Y.-F. Zhou, "High intensity focused ultrasound in clinical tumor ablation," World J. Clin. Oncol. **2**(1), 8–27 (2011).
19. F. Orsi, L. Zhang, P. Arnone, G. Orgera, G. Bonomo, P. D. Vigna, L. Monfardini, K. Zhou, W. Chen, Z. Wang, and U. Veronesi, "High-Intensity Focused Ultrasound Ablation: Effective and Safe Therapy for Solid Tumors in Difficult Locations," AJR Am. J. Roentgenol. **195**(3), W245-52 (2010).
20. M. Legay, N. Gondrexon, S. Le Person, P. Boldo, and A. Bontemps, "Enhancement of Heat Transfer by Ultrasound: Review and Recent Advances," Int. J. Chem. Eng. **2011**, 670108 (2011).
21. M. D. Brown, D. I. Nikitichev, B. E. Treeby, and B. T. Cox, "Generating arbitrary ultrasound fields with tailored optoacoustic surface profiles," Appl. Phys. Lett. **110**(9), 094102 (2017).
22. A. Vogel and V. Venugopalan, "Mechanisms of pulsed laser ablation of biological tissues," Chem. Rev. **103**(2), 577–644 (2003).
23. I. Apitz and A. Vogel, "Material ejection in nanosecond Er:YAG laser ablation of water, liver, and skin," Appl. Phys., A Mater. Sci. Process. **81**(2), 329–338 (2005).
24. P. Gregorčič, M. Jezeršek, and J. Možina, "Optodynamic energy-conversion efficiency during an Er:YAG-laser-pulse delivery into a liquid through different fiber-tip geometries," J. Biomed. Opt. **17**(7), 075061 (2012).
25. N. Lukač, J. Zadravec, P. Gregorčič, M. Lukač, and M. Jezeršek, "Wavelength dependence of photon-induced photoacoustic streaming technique for root canal irrigation," J. Biomed. Opt. **21**(7), 075007 (2016).
26. B. Cencič, P. Gregorčič, J. Možina, and M. Jezeršek, "Laser tattoo removal as an ablation process monitored by acoustical and optical methods," Appl. Phys., A Mater. Sci. Process. **112**(1), 65–69 (2013).
27. J. Mark, K. Ngai, W. Graessley, L. Mandelkern, E. Samulski, J. Koenig, and G. Wignall, *Physical Properties of Polymers, 3rd Edition* (Cambridge University Press, 2004).
28. J. Mark, (Ed.), *Physical Properties of Polymers Handbook, Second edition* (Springer-Verlag, 2006).
29. C. Li, S. Li, G. Guan, C. Wei, Z. Huang, and R. K. Wang, "A comparison of laser ultrasound measurements and finite element simulations for evaluating the elastic properties of tissue mimicking phantoms," Opt. Laser Technol. **44**(4), 866–871 (2012).
30. F. G. Pérez-Gutiérrez, R. Evans, S. Camacho-López, and G. Aguilar, "Mechanical response of agar gel irradiated with Nd:YAG nanosecond laser pulses," Proc. SPIE **7562**, 756212 (2010).
31. C. Sun, S. D. Pye, J. E. Browne, A. Janeczko, B. Ellis, M. B. Butler, V. Sboros, A. J. W. Thomson, M. P. Brewin, C. H. Earnshaw, and C. M. Moran, "The speed of sound and attenuation of an IEC agar-based tissue-mimicking material for high frequency ultrasound applications," Ultrasound Med. Biol. **38**(7), 1262–1270 (2012).
32. V. T. Nayar, J. D. Weiland, C. S. Nelson, and A. M. Hodge, "Elastic and viscoelastic characterization of agar," J. Mech. Behav. Biomed. Mater. **7**, 60–68 (2012).
33. K. Zell, J. I. Sperl, M. W. Vogel, R. Niessner, and C. Haisch, "Acoustical properties of selected tissue phantom materials for ultrasound imaging," Phys. Med. Biol. **52**(20), N475–N484 (2007).
34. H. M. Ahmed, N. M. Salem, A. F. Seddik, and M. I. El Adawy, "On shear wave speed estimation for agar-gelatine phantom," International Journal of Advanced Computer Science and Applications **7**(2), 401–409 (2016).
35. T. J. Hall, M. Bilgen, M. F. Insana, and T. A. Krouskop, "Phantom materials for elastography," IEEE T. Ultrason. Ferr. **44**(6), 1355–1365 (1997).
36. C. M. Moran, N. L. Bush, and J. C. Bamber, "Ultrasonic propagation properties of excised human skin," Ultrasound Med. Biol. **21**(9), 1177–1190 (1995).
37. M. Pawlaczyk, M. Lelonkiewicz, and M. Wieczorowski, "Age-dependent biomechanical properties of the skin," Postepy Dermatol. Alergol. **5**(5), 302–306 (2013).
38. R. Petkovšek, P. Gregorčič, and J. Možina, "A beam-deflection probe as a method for optodynamic measurements of cavitation bubble oscillations," Meas. Sci. Technol. **18**(9), 2972–2978 (2007).
39. R. Petkovšek and P. Gregorčič, "A laser probe measurement of cavitation bubble dynamics improved by shock wave detection and compared to shadow photography," J. Appl. Phys. **102**(4), 044909 (2007).
40. P. Gregorčič, R. Petkovšek, J. Možina, and G. Močnik, "Measurements of cavitation bubble dynamics based on a beam-deflection probe," Appl. Phys., A Mater. Sci. Process. **93**(4), 901–905 (2008).
41. P. Gregorčič, J. Diaci, and J. Možina, "Two-dimensional measurements of laser-induced breakdown in air by high-speed two-frame shadowgraphy," Appl. Phys., A Mater. Sci. Process. **112**(1), 49–55 (2013).
42. P. Gregorčič, N. Lukač, J. Možina, and M. Jezeršek, "Synchronized delivery of Er:YAG-laser pulses into water studied by a laser beam transmission probe for enhanced endodontic treatment," Appl. Phys., A Mater. Sci. Process. **122**(4), 459 (2016).
43. J. Diaci, "Response Functions of the Laser-Beam Deflection Probe for Detection of Spherical Acoustic-Waves," Rev. Sci. Instrum. **63**(11), 5306–5310 (1992).
44. D. T. Sandwell, "Biharmonic spline interpolation of GEOS-3 and SEASAT altimeter data," Geophys. Res. Lett. **14**(2), 139–142 (1987).

Biomedical Optics EXPRESS

45. X. Deng and Z. Tang, "Moving surface spline interpolation based on Green's function," Math. Geosci. **43**(6), 663–680 (2011).

## 1. Introduction

Laser-based diagnostics and treatments have been present in medical science in last two decades with desired medical results achieved by primary light absorption effects [1–7]. The secondary effects of such a vigorous light-matter interaction in the form of laser-induced elastic transients, including ultrasound, propagating through the undulating tissue are gaining in attention and practical use, either to explore new aspects in their application or to prevent excessive damage to the tissue. The many aspects of optical investigations of the mechanical properties of biological tissue by measuring its deformations in response to a stimulus are also explored in the growing field of optical elastography [8–13]. Even though much is understood about elastic wave propagation in soft matter in general [14,15], the research of laser-induced elastic waves in soft tissue remains scientifically and commercially an interesting topic as their potential benefits have yet to be profoundly explored and developed [16–21]. Much of the research was focused on occurrences on the laser-illuminated substrate surface and the ablation plumes ejected from it [22,23], while laser-induced elastic wave propagation deeper within the substrate was largely missed—one can hardly find an optical high-speed camera recording of particle movements during wave transitions in soft matter in the literature, for example. With an interest in developing laser-based, non-invasive sub skin procedures, we conducted a preliminary research on laser effects on skin phantoms and laser-induced elastic transients propagating inside. In all, the questions about such aspect as fluence damage thresholds on the surface and in depth, area effects, depth of penetration, and effects of elastic transient within the tissue remain open and need to be addressed.

The use of a laser pulse as a stimulating source in elastic media offers some advantages over mechanical stimulants as it is non-contact and enables easy control over its temporal and spatial distributions, energy, and momentum. It also enables a study of light-matter interactions and their consequences. The usual laser-induced mechanisms based on energy absorption in the illuminated volume employed in medicine are surface ablation, internal cavitation, thermal expansion, and chemical transformation. Each of these interactions also produces its own distinct elastic transient waves in the affected tissue. For surface treatments, Er:YAG lasers are mostly used as they emit light at the wavelength of 2940 nm which is highly absorptive in the water-containing tissue [1–5,24,25]. Nd:YAG lasers are commonly used for deeper tissue penetration, as the water is mostly transparent for their light at the wavelength of 1064 nm while it is easily absorbed in other media such as pigments or ink [1–6,26].

As a soft polymeric gel, agar, traditionally used as a nutrient in human cuisine and in microbiological work, was found to be an adequate organic soft tissue substitute. As it exhibits elastic properties close to most soft tissues, including skin, it is a good first approximation for them *in vitro* [22–37]. From experimental viewpoint, the advantage of such a water-based soft tissue phantom is mainly that it is translucent in the visible part and highly absorptive in the infrared part of the light spectrum. This allows us to directly observe the occurrences inside while still stimulating it with appropriate light pulses without contact.

When such a water-abundant substance is illuminated by a highly-absorptive laser pulse of sufficient energy and duration, the quickly absorbed energy is mostly converted into ablation with the reactive force of the expelled material launching elastic transients throughout the bulk of the substrate. Fast material expulsion at high energies, through a large momentum transfer, induces mechanical waves [22,23] that are relatively slow and have high amplitudes. At high enough energies, large laser-induced bubbles [38–40] are formed near the substrate surface while, through ablation and tearing, damage is incurred. Another type of waves to be observed are ultrasonic transients [29,31,36] which are relatively fast and have much smaller amplitudes. They are launched by very short stimulating pulses such as

Biomedical Optics EXPRESS

prominent spikes protruding out of a jagged power profile of a longer stimulating laser pulse. As these two distinct mechanical wave-types, induced by the same laser pulse, differ by several orders of magnitude in terms of their propagation velocity and amplitude, they may be well separated from each other, if their modes of detection and measuring instruments are chosen accordingly.

While detection of ultrasonic transients requires very fast probing techniques [41], a large field of view is preferred for observation of ablation-induced elastic waves. The laser-beam-based probes provide a cumulative line information about the translucent material based on the change of its refractive index with very fast response times to any perturbations [38,39,42]. The high-speed camera, though usually not as fast as the probe and too slow to directly capture ultrasonic wave propagation but with much greater spatial resolution, records visual information in a limited two-dimensional field of view during fast events. They both offer a novel insight into the occurrences during the interaction of the stimulating laser pulse and the soft matter as well as during the elastic wave propagation and reverberation.

In this paper, we present an experimental examination of Er:YAG-light-matter interactions and laser-induced elastic wave propagation in agar soft tissue phantoms within the parameters of the normal clinical use of such laser systems. It may serve as a foundation of this kind of optical *in vitro* investigating techniques for (bio)medical purposes. Since the laser ablation itself, laser bubble formations and laser damages to the surface have already been covered extensively [22,23,26,38–40], we focused on occurrences deeper in the substrate with new analytical approach. Optical measurement and analysis of elastic wave propagation was conducted in two parts. First, as a viable way of determining its elastic properties and to inform their potential comparisons with different substrates, we measured the propagation velocity of the ultrasonic pressure waves in agar gel with a laser-beam-deflection probe (LBDP). Second, directly observing with a high-speed camera, we recorded particle displacements during laser-induced elastic wave transition in agar gel with a sparse population of hollow glass spheres marking particular points. We employed a custom developed image recognition and velocimetry algorithms to extract time-dependent particle movement information from the recordings. From the acquired particle displacements and trajectories, the temporal displacement, strain and amplitude fields showing the transition of ablation-induced elastic transients were interpolated as well. Evaluated from the recordings were also damages sustained by single and repeated laser-ablation interactions.

## 2. Methods

### *2.1 Ultrasound propagation measurements with a laser-beam-deflection probe*

Three batches of commercially available culinary agar powder dissolved in boiling water in mass concentrations of 20 ± 1 g/L were set in open rectangular glass containers with dimensions of 50 mm x 25 mm x 27 mm and wall thickness of 1.8 mm. Transparent containers ensured a constant volume and a constant shape of the gel inside them while their smooth surfaces provided a clear optical path for the light entering and exiting through their walls.

As mechanical waves are propagating compressions and rarefactions of matter in a medium that cause transient changes of the local refractive index [43], the propagation velocity of the ultrasonic pressure waves was measured by the LBDP in an experimental setup presented in Figs. 1(a) and 1(b).

The agar gel in an open glass container was stimulated on its top surface by microsecond laser pulses, one per each measurement, generated by an Er:YAG laser (AT Fidelis, Fotona, Slovenia) with the wavelength of 2940 nm. The normally incoming pulses had a roughly uniform circular surface distribution with a diameter of 1.9 mm as determined by measuring their imprints on a photographic paper under experimental conditions. Their time profile, while in the approximate shape of an asymmetric bell with a width of 100 μs (measured at 10% of average pulse power), contained some distinct short peaks with an average full width

Biomedical Optics EXPRESS

at half maximum of 0.5 μs that were short enough to launch ultrasonic waves. These peaks are visible in the green curves in Figs. 1(c) and 1(d), where just the beginning of the entire laser pulse is shown. Typical power evolution of free-running Er:YAG laser pulses can be found elsewhere [24].

At a certain depth, $z$, directly beneath the laser-stimulated spot, a continuous-wave He-Ne laser beam (05-LHP-141, Melles Griot, USA; wavelength 632.8 nm) with a beam diameter of 1.0 mm was irradiating through the substrate onto a quadrant photodiode (rise time ~4 ns, bandwidth ~200 MHz) placed on the other side. When the optical path of the probing beam was crossed by a passing mechanical wave, such transient change in the refractive index caused a deflection of the beam from its unperturbed direction. This deflection was detected in two orthogonal directions as a change in the incoming beam intensity by the quadrant photodiode. With a sampling frequency of 500 MHz, its vertical deflection signal was recorded by an oscilloscope (WaveRunner 64MXi-A, LeCroy, USA; bandwidth 600 MHz, maximum sampling rate 10 GS/s) which simultaneously recorded a signal from a 60-MHz InAs photodiode that was set to detect the intensity of the stimulating (Er:YAG) laser pulse. Such typical signals, unfiltered and low-pass-filtered (8th order with cutoff at 2.5 MHz), are shown in Figs. 1(c) and 1(d). From both signals, the delay, $t_z$, between the irradiation from the stimulating pulse and the initial perturbation of the probing beam by the arrival of the first ultrasonic wave was measured. For each measurement, the probing beam was set at two depths beneath the surface: $z_1$ = 3.5 mm and $z_2$ = 17.0 mm, giving two time delays: $t_{z1}$ and $t_{z2}$, which give the propagation velocity of the ultrasonic pressure waves:

$$c_P = \frac{z_2 - z_1}{t_{z2} - t_{z1}}. \tag{1}$$

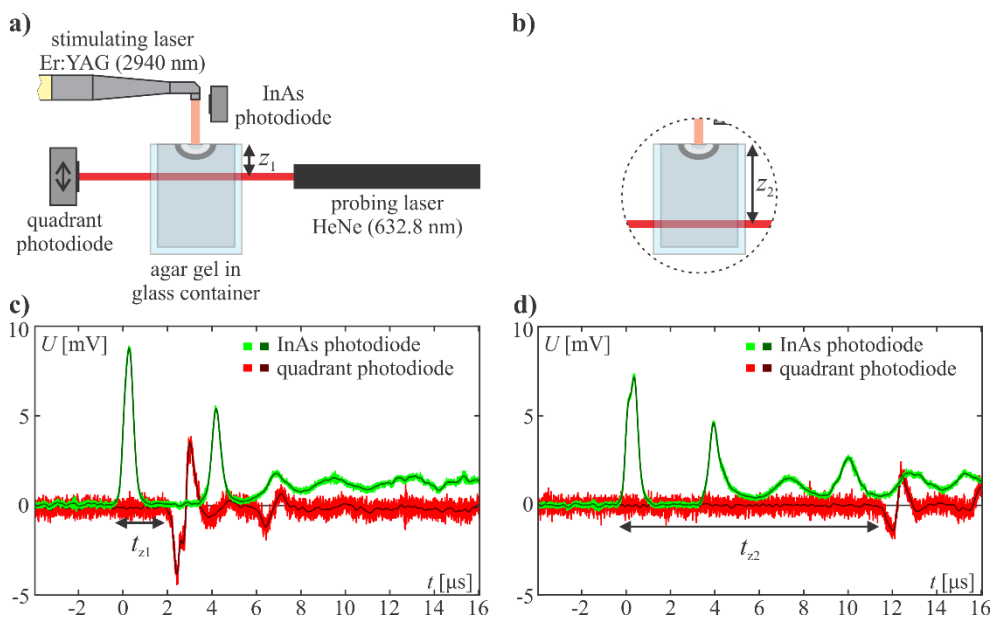


Fig. 1. Schematics of the LBDP setup for measuring the propagation velocity of the ultrasonic pressure waves in agar blocks at two probing depths: (a) $z_1$ and (b) $z_2$. Representative signals (unfiltered and low-pass-filtered) from InAs (green) and quadrant (red) photodiodes, measuring the intensities of the stimulating pulse and the LBDP beam, respectively, at both probing depths: (c) $z_1$ and (d) $z_2$. From them, the temporal delays $t_{z1}$ and $t_{z2}$ between the stimulation and detection of the first ultrasonic transient are measured.

Biomedical Optics EXPRESS

### 2.2 Internal displacements recorded with a high-speed camera

For internal particle movement recording with a high-speed camera, a single batch of agar gel was produced similarly as in the LBDP experiment and set into the same glass containers. Agar powder in mass concentration of 20 ± 1 g/L was dissolved in water to which hollow borosilicate glass spheres with an average diameter of 10 μm were added in mass concentration of 1.8 g/L. Since their mass density of 1.1 g/cm$^3$ is similar to that of the set gel, their population was distributed randomly with an average particle density estimated at about 240 spheres/mm$^3$ and an average distance between the closest spheres of about 0.1 mm. The spheres are transparent for the excitation Er:YAG light but when they were illuminated by a white light each sphere served as a visual shadow marker for a specific point in the substrate. Although they are many, the spheres were distributed sparsely enough so they did not obstruct the propagation of light significantly more than did the diffusive nature of agar gel itself as clear images of the spheres were obtained from the middle of the agar blocks.

In the recording setup, agar gel in an open glass container was stimulated similarly as in the LBDP experiment. Short laser pulses, one per each measurement, generated by an Er:YAG laser were incoming normally on the top surface of the agar block. The pulses had a roughly uniform circular surface distribution with a diameter of 2.0 mm and the same time profile as in LBDP experiments, while the pulse energies ranged from 100 mJ to 400 mJ. The substrate was illuminated from the back side by a bright white light and the high-speed camera (FASTCAM SA-Z, Photron, Japan) was used for the shadowgraphic recordings on the front, as illustrated in Fig. 2(a). It was focused on the vertical focal plane set within the gel 10 mm from its front side in line with the laser incident plane. A micro objective with a 5x magnification, a focal length of 40 mm, and depth of field of 14 μm attached to the camera made the size its field of view 4.1 mm x 4.1 mm in the focal plane. The recording frequency at the full resolution of 1024 x 1024 pixels was capped at 20,000 fps. The usual recordings were composed of 501 images in overall duration of 25 ms. The camera was computer controlled and triggered by an InAs photodiode that was set to detect the light from the stimulating laser pulse. With it, the time designation at the moment of laser pulse impact was set to $t = t_0 = 0$ ms.

In a variation of the setup, the propagation of laser-induced elastic waves on the agar surface was also recorded in a manner presented in Fig. 2(b).

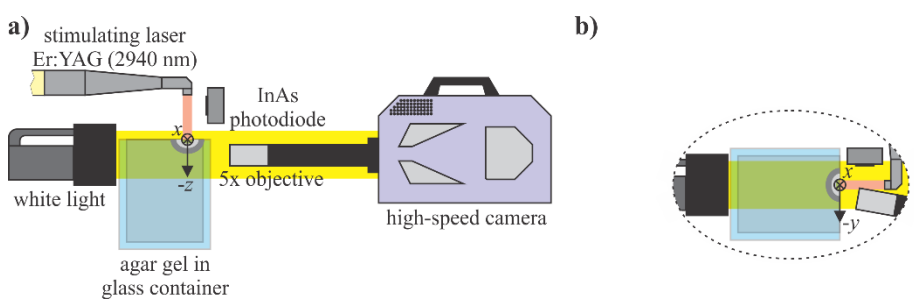


Fig. 2. Schematics of the high-speed-camera setup for recording the laser-stimulated mechanical wave propagation (a) inside the agar blocks and (b) on their surface.

In the recordings of ablation-induced transients inside the agar gel, randomly dispersed glass spheres were identified and tracked with a custom developed image recognition algorithm written in LabView utilizing the methods of particle image velocimetry (PIV). With set size, contrast and distance parameters, this processing algorithm recognizes each individual particle in each image in a recording, records its position in two orthogonal directions: $z(t_j)$ (longitudinal) and $x(t_j)$ (lateral), and associates this information from consecutive images into a trajectory ($x(t)$, $z(t)$) and displacement components: $u_z(t) = z(t) - z(t_0)$ and $u_x(t) = x(t) - x(t_0)$, while discarding incomplete and residual data. The obvious

Biomedical Optics EXPRESS

artificial outliers produced by the algorithm were filtered out by means of the nearest credible value approach. From this, a mesh of evenly distributed points was interpolated for each frame by means of biharmonic spline interpolation [44,45] to reveal the time-dependent, two-dimensional point displacement mesh undulating during the laser-induced elastic wave transition. From these, the temporal material deformations were calculated in the form of a relative strain:

$$e_{\mathrm{i}}^{\mathrm{REL}}(t_{\mathrm{j}}) = \frac{u_{\mathrm{i+1}}(t_{\mathrm{j+1}}) - u_{\mathrm{i}}(t_{\mathrm{j+1}})}{u_{\mathrm{i+1}}(t_{\mathrm{j}}) - u_{\mathrm{i}}(t_{\mathrm{j}})}. \tag{2}$$

Equation (2) defines a ratio of the distances between two neighboring points in a mesh as they are displaced by a transient $u_{\mathrm{i}+1}(t)$ and $u_{\mathrm{i}}(t)$ at two successive time points $t_{\mathrm{j}}$ and $t_{\mathrm{j}+1}$. A further analysis of the interpolated displacement data was done to evaluate local displacement peak-to-peak amplitudes (maximum local displacement range) during laser-induced elastic wave transitions to indicate the overall distribution of elastic energy. Their suprema (maximum amplitudes overall) were also evaluated in correlation to the stimulating pulse energies.

## 3. Results

### *3.1 Ultrasound propagation measurements with a laser-beam-deflection probe*

The measurements of ultrasonic wave transitions were conducted on three batches of agar skin phantoms. The agar mass concentration $\rho_{\mathrm{agar}}$ slightly varies ( ± 5%) due to not perfectly repeatable procedure for preparation. During these measurements, we used two different nominal laser pulse energies $E_{\mathrm{N}}$. In each of the three sets of measurements, we performed five repetitions resulting in a limited spread of calculated propagation velocities $c_{\mathrm{P}}$ as presented in Table 1. The noticeable dissimilarity in propagation velocities between agar gel batches is likely subject to the deviation in agar concentrations in the samples. From results in Table 1, we can conclude that the speed of sound in agar gel equals to about 1.46 km/s; this value is very similar to the speed of sound in water.

**Table 1. Propagation velocities of ultrasonic pressure waves in agar gel skin phantoms.**

| $\rho_{\mathrm{agar}}$ [g/L] | $E_{\mathrm{N}}$ [mJ] | $c_{\mathrm{P}}$ [m/s] |
|---|---|---|
| 20 ± 1 | 400 | 1423 ± 33 |
| | 150 | 1505 ± 43 |
| | 150 | 1449 ± 41 |

### *3.2 Internal displacements recorded with a high-speed camera*

For each of the setup variations, the representative sequence of recorded images is presented in Fig. 3. Laser-induced bubble formation and collapse within the substrate are shown in Fig. 3(a). It was observed that the bubble reaches its maximum radius of 1.5 mm, while its oscillation time equals 2.0 ms. Figure 3(b) shows laser-induced surface wave propagation and surface material damage. Both phenomena have been intensively examined and discussed elsewhere [22,23,26,38–40]; therefore, they are mentioned here for illustration purposes only.

Movement and software tracking of glass spheres as shadow objects inside the substrate during the laser-ablation-induced elastic wave transition is presented in Fig. 3(c). These images are enlarged cutouts from larger shadowgraphic images with their position marked by a dashed rectangle in Fig. 4(a). The idea of the tracking algorithm is demonstrated on the example of two particles, circled at $t = 0$ ms. Note that during recording images were acquired each 50 µs, but only 0th (at 0 ms), 40th (at 2 ms), 120th (at 6 ms), and 500th (at 25 ms) images are shown here. The yellow curve shows the path travelled by a selected particle in time between the successive images presented here, while its cumulative path is marked by the red curve.

Biomedical Optics EXPRESS

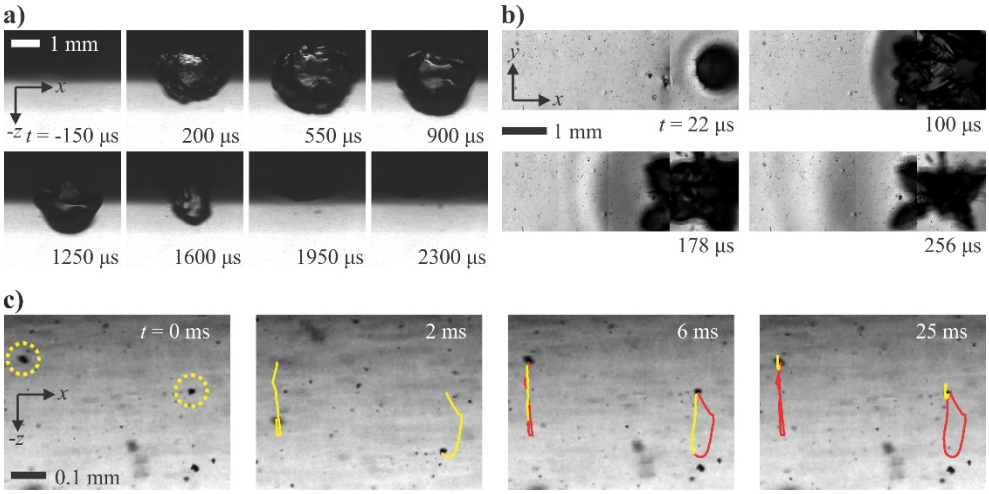


Fig. 3. Typical image sequences of (a) laser-induced bubble formation and collapse inside the agar blocks at pulse energy of 400 mJ; and (b) propagation of laser-induced elastic waves on agar surface and laser-incurred surface material damage at pulse energy of 150 mJ. (c) Selected cutouts of shadowgraphic images of glass spheres used for their movement tracking during elastic wave transitions as induced by a 200 mJ laser pulse.

An interpolated mesh of point trajectories induced by a 200 mJ laser pulse and acquired by the image recognition algorithm utilizing the PIV methods and spline interpolation is presented in Fig. 4(a). Four typical trajectories ($u_x(t)$, $u_z(t)$) and their time-dependent orthogonal displacement components $u_z(t)$ (longitudinal) and $u_x(t)$ (lateral) in four distinct positions, labeled b–e in Fig. 4(a), relative to the laser-illuminated area are enlarged in Figs. 4(b)–4(e).

Biomedical Optics EXPRESS

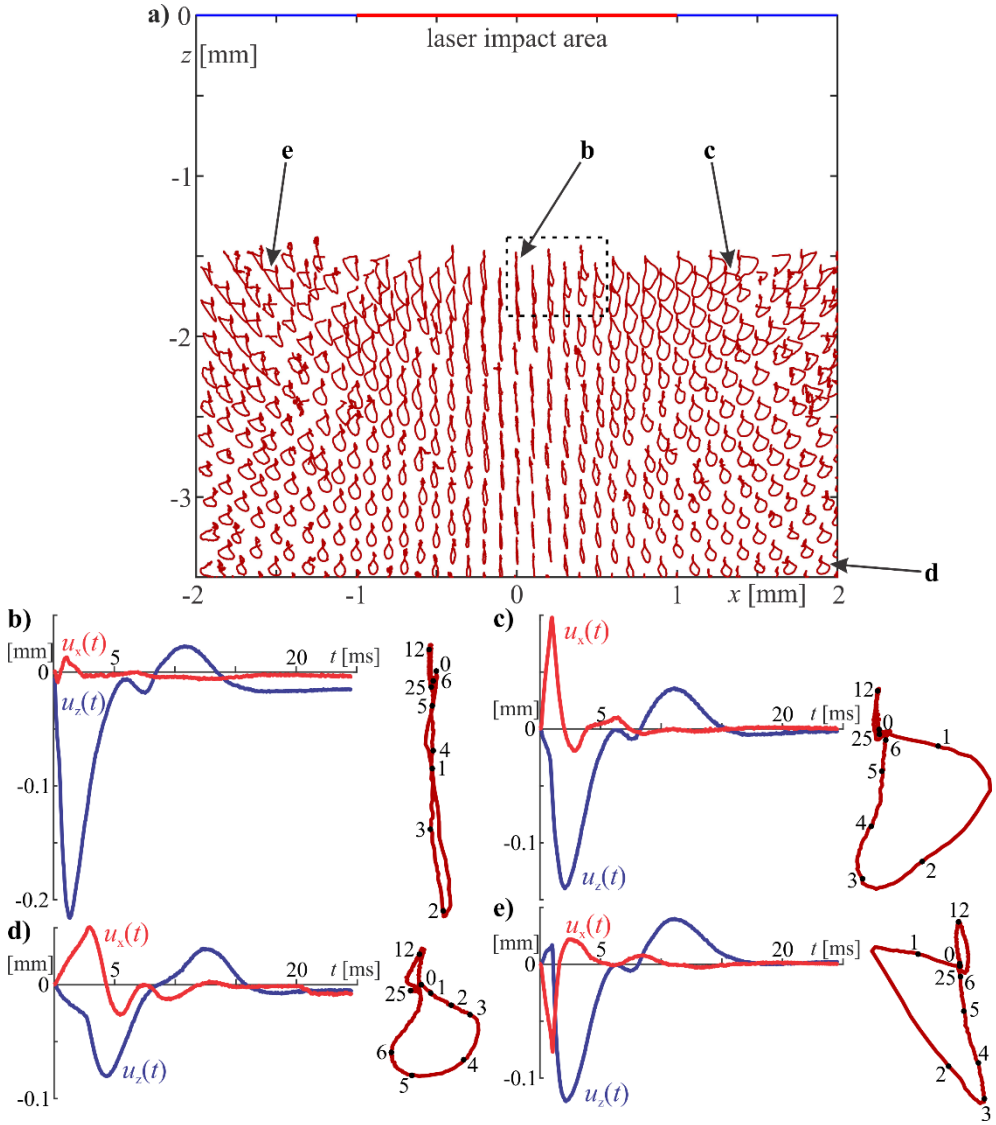


Fig. 4. (a) A mesh of point trajectories was acquired by the image recognition algorithm utilizing the PIV methods and spline interpolation from a single particle displacement recording during elastic wave transitions as induced by a 200 mJ laser pulse in duration of 25 ms (501 frames). Enlarged are (b)–(e) four typical trajectories ($u_x(t)$, $u_z(t)$), with marked time points in milliseconds, on the right-hand side of the graphs showing their time-dependent orthogonal displacement components $u_z(t)$ (longitudinal) and $u_x(t)$ (lateral) in four distinct positions relative to the laser-illuminated area.

Figure 5(a) demonstrates a representative time-dependent transition of ablation-induced elastic waves caused by a 200 mJ laser pulse in a sequence of linearly interpolated color-coded absolute material displacement fields for each of the two orthogonal directions, separately. In Fig. 5(b), the same event is also presented as a sequence of linearly interpolated color-coded temporal fields of relative strain for each of the two orthogonal directions, separately. Due to the nature of field calculations, the displacements and deformations at time $t$ = 0 ms are, in general, equal to zero with an additional level of stochastic and systemic background noise present.

Biomedical Optics EXPRESS

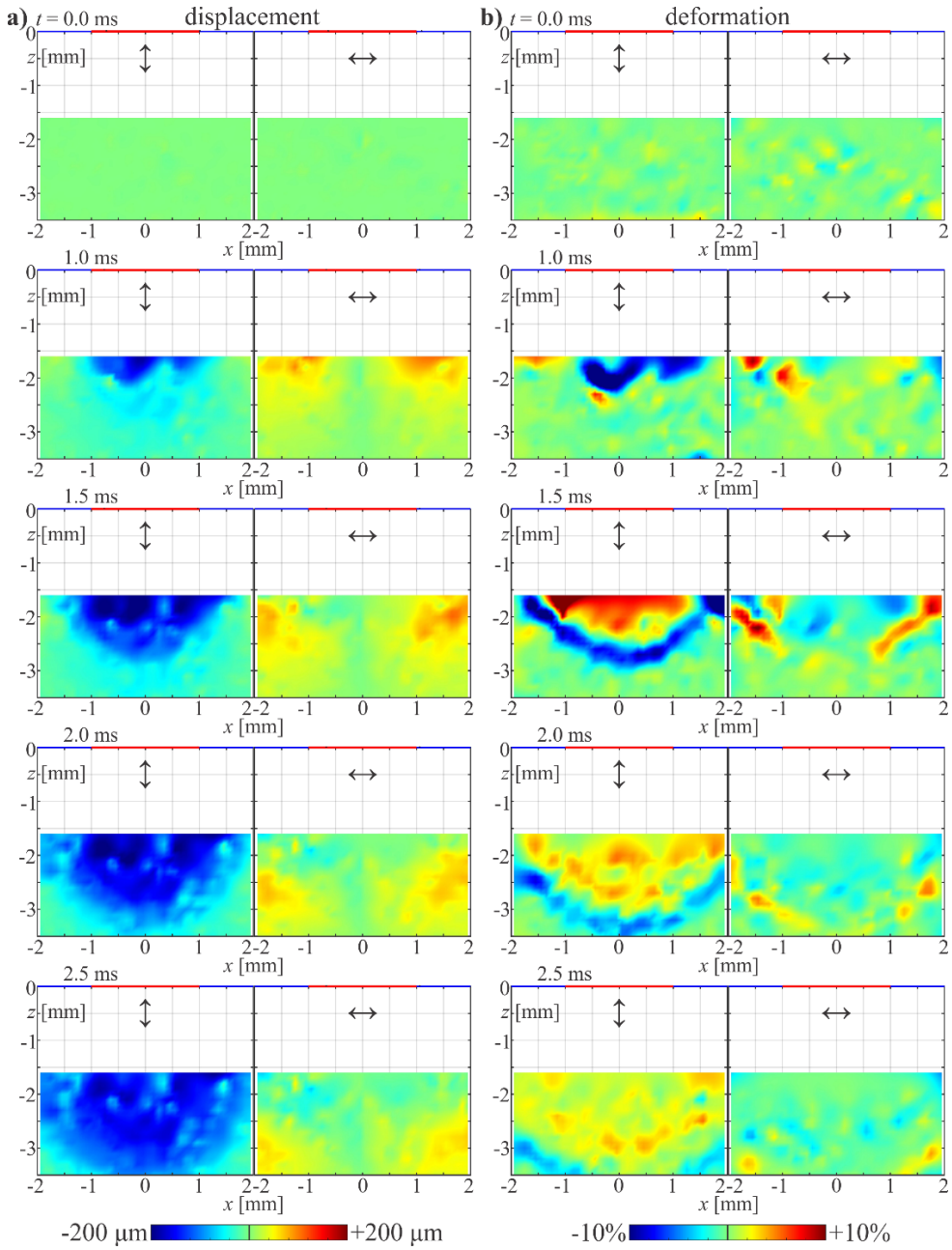


Fig. 5. Transition of ablation-induced elastic waves after irradiation by a 200 mJ laser pulse shown (a) in absolute material displacement fields and (b) as temporal material deformations in fields of relative strain. Results are shown for longitudinal ↕ (left) and lateral ↔ (right) directions at five time points, separately.

Local displacement amplitudes are presented in Fig. 6 as linearly interpolated color-coded displacement amplitude fields for each of the two perpendicular directions at four stimulating laser pulse energies, ranging from 100 mJ to 400 mJ, with different corresponding amplitude suprema $u_{SUP}$.

Biomedical Optics EXPRESS

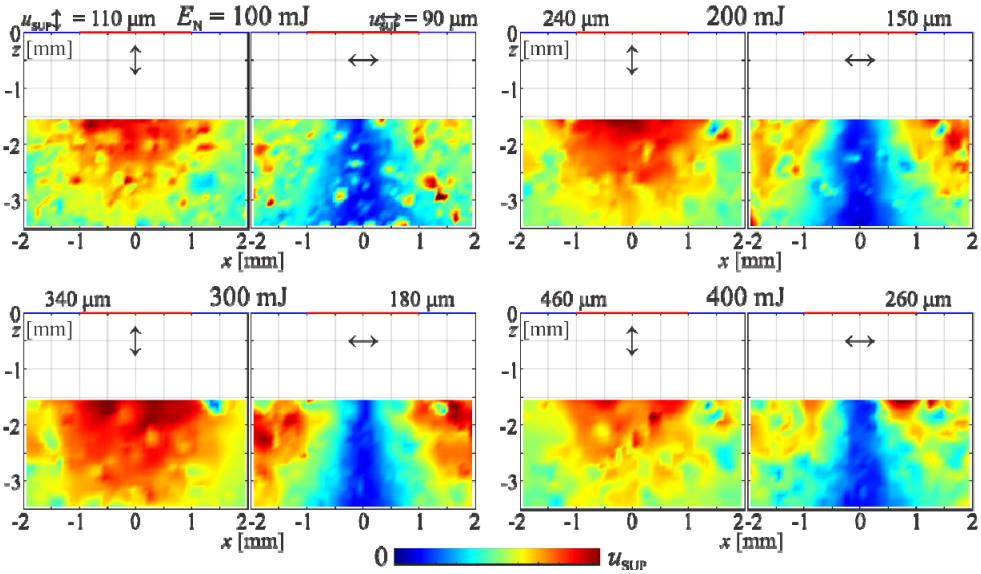


Fig. 6. Linearly interpolated color-coded local displacement amplitude fields showing longitudinal ↕ (left) and lateral ↔ (right) displacement amplitudes separately at four stimulating pulse energies $E_N$ with different corresponding amplitude suprema $u_{SUP}$. They indicate the overall distribution of the elastic energy pertaining to each displacement direction.

The amplitude suprema of both perpendicular displacement directions at each stimulating pulse energy are plotted in Fig. 7. A linear function $u_{SUP} = k\ E_N$ was fitted to them whose coefficients for longitudinal and lateral suprema are $k_{long}$ = 1.15 mm/J and $k_{lat}$ = 0.66 mm/J, respectively. At stimulating pulse energies higher than about 400 mJ, considerable external and internal laser-incurred damage was observed in the agar gel samples.

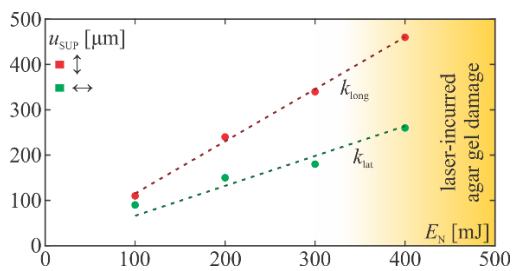


Fig. 7. Plot of longitudinal ↕ (red) and lateral ↔ (green) displacement amplitude suprema $u_{SUP}$ corresponding to four stimulating pulse energies $E_N$ with a linear function fitted to each of them.

## 4. Discussion

Direct optical observation of laser-gel interaction provided by the high-speed camera recordings is used to study the effects of stimulating pulse energy as well as its spatial and temporal distributions on dramatic events, such as laser-induced bubble formation and material damage as well as subtler occurrences in the form of ablation-induced mechanical wave propagation through the substrate. Faster and even more delicate events, such as laser-induced ultrasound propagation, are detected by the LBDP.

As a rudimental soft tissue substitute, agar gel proves to be reasonably well suited for *in vitro* experimentation with its transparency in visible part of light spectrum enabling the employment of even the simplest optical investigative methods. Since it is based on water, which is highly absorptive for light at the wavelength of 2940 nm, the Er:YAG lasers are well suited for surface and near-surface interactions. Experimental aspects of skin phantoms can

Biomedical Optics EXPRESS

be greatly expanded with the addition of appropriate particles or even ink, either in layers, capillaries, small bubbles or dispersed in the bulk of the substrate. The latter would prove invaluable in studying the accompanying mechanical mechanisms during laser tattoo removal, for example, where Nd:YAG lasers of the wavelength of 1064 nm would be more suitable.

As the agar gel was illuminated by the Er:YAG laser pulses with energies of the order of magnitude of 100 mJ, the quick energy absorption caused surface ablation that lasted milliseconds. Such fast material expulsion induced significant elastic transients that propagated through the bulk of the substrate. It was measured that ablation-induced mechanical waves had propagation velocities of about 1 m/s with displacement amplitudes of the order of magnitude of 0.1 mm. At higher energies, the formation of large laser-induced bubbles near the substrate surface was observed, as shown in the sequence in Fig. 3(a), while the ablation and tearing damage at similar energies is shown in Fig. 3(b). The ultrasonic transients were measured to propagate at velocities of about 1.46 km/s, as presented in Table 1. They had, in estimation, about three orders of magnitude smaller displacement amplitudes as their ablation-induced counterparts. They were found to have been launched by prominent microsecond spikes protruding out of the overall power profile of the stimulating laser pulse, seen in Figs. 1(c) and 1(d), with each micro pulse amounting to only a small portion of the entire stimulating energy; about one thousandth, in estimation.

Since a single probing laser beam substantially limits its spatial resolution, the LBDP is best used for measuring time intervals between significant events. Its advantage in this case, however, is in its fast responsiveness enabling it to capture fast transient phenomena [40]. Although the principles of measuring the propagation velocity of the ultrasonic pressure waves $c_P$ with such a probe are quite simple, the results of around 1.42 km/s to 1.51 km/s are comparable with results from the literature for agar gel [27–35] and skin [22,23,36,37]. The latter further indicates that agar gel may indeed be used as a rudimental skin substitute given that its density is also similar to that of skin [22,23,36,37]. From such information, other moduli pertaining to elastic properties of the substrate including propagation dispersion and attenuation may be further inferred as well [14,15].

From individual particle time-dependent displacements provided by the analysis of the high-speed camera recordings, as exemplified in Figs. 4–6, the ablation-induced elastic transient propagation can be observed and decomposed. Directly under the laser pulse impact area, the material displacement is mostly in the longitudinal direction, i.e., in the direction of the laser pulse impact and opposite of the material ejection during surface ablation, while to the sides, due to the substrate being a soft solid, a strong lateral displacement component is present as well. Overall, the longitudinal displacements during the laser-induced elastic wave propagation are manifested in an expanding hemisphere beneath the laser impact area. The lateral displacements are manifested in an expanding toroidal space on all sides of the laser impact area travelling along its longitudinal axis, thus, creating a longitudinal funnel in the middle while maintaining axial symmetry. As seen in Fig. 4, the interpolated point trajectories beneath the impact area are nearly linear in shape, those to the side of it are triangular, while those deepest and furthest are almost circular. Interesting to note here is that the initial energetic transient is followed by another, weaker and slower, that displaces material in the direction opposite of the first one. Dynamically, directional material deformations mostly correspond to its displacements, as demonstrated in Fig. 5, while mirroring each other over the axial line before smoothly returning to their initial positions. From the displacement amplitude fields in Fig. 6, in accordance with previous observations, an indication of the overall distribution of elastic energy may be extracted as pertaining to each of the orthogonal displacement directions. As the stimulating laser-pulse energy was increased, a proportional increase in displacement amplitudes and their suprema was observed as displayed in the plot in Fig. 7. Beyond the stimulating laser pulse energy of about 400 mJ considerable external

Biomedical Optics EXPRESS

and internal laser-incurred damage was observed as the elastic regime of the agar gel transitions into plastic deformation and laser-incurred damage regimes.

A certain amount of noise and artefacts was present in the measurements and, although filtered, their residue was, in parts, expanded with subsequent interpolations.

## 5. Conclusions

As in-depth research of laser-induced elastic wave propagation and laser-incurred material damage for (bio)medical purposes gains in utility and significance, we demonstrated how may certain optical methods, namely laser-beam-deflection probe and high-speed camera recording with image recognition analysis, be applied to garner insight into laser-stimulated occurrences in soft tissue phantoms, such as agar gel, *in vitro*. In it, the propagation velocities of ultrasonic pressure waves were measured within the range of 1.42–1.51 km/s, as expected. This proves that agar gel may be used as a rudimental skin substitute for further investigation of laser-induced medical treatments. By embedded particle tracking in optical high-speed camera recordings, the intricate inner dynamics during transition of laser-ablation-induced elastic waves was obtained. We clearly presented distinct motion and its variation relative to the laser impact area. Our results lead to conclusion that ablation-induced mechanical waves propagate much slower than ultrasonic-pressure waves, with velocities of around 1 m/s. Their displacement amplitudes of 0.1 mm were estimated at three orders of magnitude larger than those in ultrasonic-wave propagation. Presented results offer an insight that is important for understanding of laser-induced elastic transients in soft tissue phantoms, while the methods described here provide a base for further research of laser-induced mechanical effects deeper in the soft tissue for such applications as medical diagnosis and treatments.

## Funding

Slovenian Research Agency (P2-0392).

## Acknowledgments

The authors wish to thank Fotona d. o. o. (www.fotona.com) for providing the laser system used in this research.

## Disclosures

The authors declare that there are no conflicts of interest related to this article.